Histol Histopathol (2012) 27: 1163-1174
DOI: 10.14670/HH-27.1163

http://www.hh.um.es

Histology and Histopathology
Cellular and Molecular Biology

The extent of ultrastructural spinal cord pathology reflects disease severity in experimental autoimmune encephalomyelitis

Traugott L. Gruppe, Mascha S. Recks, Klaus Addicks and Stefanie Kuerten
Department of Anatomy I, University of Cologne, Germany

Summary. Experimental autoimmune encephalomyelitis (EAE) has been studied for decades as an animal model for human multiple sclerosis (MS). Here we performed ultrastructural analysis of corticospinal tract (CST) and motor neuron pathology in myelin oligodendrocyte glycoprotein (MOG) peptide 35-55- and MP4-induced EAE of C57BL/6 mice. Both models were clinically characterized by ascending paralysis. Our data show that CST and motor neuron pathology differentially contributed to the disease. In both MOG peptide- and MP4-induced EAE pathological changes in the CST were evident. While the MP4 model also encompassed severe motor neuron degeneration in terms of rough endoplasmic reticulum alterations, the presence of intracytoplasmic vacuoles and nuclear dissolution, both models showed motor neuron atrophy. Features of axonal damage covered mitochondrial swelling, a decrease in nearest neighbor neurofilament distance (NNND) and an increase of the oligodendroglial cytoplasm inner tongue. The extent of CST and motor neuron pathology was reflective of the severity of clinical EAE in MOG peptide- and MP4-elicited EAE. Differential targeting of CNS gray and white matter are typical features of MS pathology. The MOG peptide and MP4 model may thus be valuable tools for downstream studies of the mechanisms underlying these morphological disease correlates.

Key words: CNS histopathology, Corticospinal tract, EAE, Motor neuron, MS

Offprint requests to: Stefanie Kuerten, Department of Anatomy I, University of Cologne, Joseph-Stelzmann-Str. 9, 50931 Cologne, Germany. e-mail: stefanie.kuerten@uk-koeln.de

Introduction

Multiple sclerosis (MS) is considered to be a chronic inflammatory disease of the central nervous system (CNS), characterized by multifocal, disseminated inflammation, demyelination, axonal damage and gray matter pathology (Bitsch et al., 2000; Lassmann et al., 2007; Calabrese et al., 2010). The etiology and pathogenetic mechanisms underlying MS have remained unclear and a limited access to human tissue samples has made extensive histological studies difficult to perform (Gold et al., 2006). To this end, experimental autoimmune encephalomyelitis (EAE) has been established as an animal model for MS (Goverman and Brabb, 1996; Sospedra and Martin, 2005; Steinman and Zamvil, 2006; Handel et al., 2011). EAE can be induced either by active immunization with CNS antigens or by the passive transfer of encephalitogenic T cells into susceptible animal strains. In particular, the C57BL/6 (B6) mouse strain is frequently used since most gene-modified mice are generated on this background. Traditional models on the B6 background include the myelin oligodendrocyte glycoprotein (MOG) protein- and peptide 35-55- (Mendel et al., 1995; Bernard et al., 1997; Oliver et al., 2003), as well as the proteolipid protein (PLP) peptide 178-191-induced EAE (Tompkins et al., 2002; Kuerten et al., 2006). We have recently introduced MP4-elicited EAE, relying on a myelin basic

Abbreviations: CNS, central nervous system; CST, corticospinal tract; EAE, experimental autoimmune encephalomyelitis; rER, rough endoplasmic reticulum; MBP, myelin basic protein; MOG, myelin oligodendrocyte glycoprotein; MOGp, MOG peptide 35-55; MP4, MBP-PLP fusion protein; MS, multiple sclerosis; NNND, nearest neighbor neurofilament distance; PLP, proteolipid protein; TRAIL, TNF-related apoptosis inducing ligand

protein (MBP)-PLP fusion protein. We have pointed out the benefits of working with this model in our previous publications (Kuerten et al., 2006, 2007, 2008, 2011a).

The advantage of investigating the development of EAE in a single mouse strain resides in a better comparability of the results - this approach allows tracing back the differences between the models to the immunization with the CNS antigen while excluding genetic diversity. In our previous studies we have delineated differences in CNS inflammation, demyelination, axonal damage and motor neuron atrophy induced by MOG peptide 35-55 (MOGp), PLP peptide 178-191 and MP4 (Kuerten et al., 2006, 2008, 2011b). We have shown that MP4-induced EAE was characterized by differential infiltration of CNS regions in addition to dynamic lesion composition that allowed the histological staging of the disease. In contrast, the MOG peptide model displayed static patterns of inflammation, while there were no classifiable patterns in the PLP peptide model. Demyelination was transient in MOG peptide-elicited EAE, chronic in the MP4 and absent in the PLP peptide model. Axonal damage evaluated by SMI-32 immunostaining was comparable in the three models suggesting this feature as a morphological correlate for chronic clinical deficits in the mice.

An intriguing difference between MOG peptide and MP4-induced EAE included the differential targeting of spinal cord motor regions. While in the MOG peptide model CST pathology was evident, MP4-induced EAE was rather characterized by motor neuron alterations. However, all of our previous studies relied on light microscopic analysis (Kuerten et al., 2011b; Recks et al., 2011), which can give a general overview of the pathologic traits of each model, while falling short in providing details about the fine characteristics of nerve fiber and neuronal damage. In the present study, we extended our analysis to include electron microscopy and we aimed at delineating the potentially differential causes of functional motor deficits in the MOG peptide and MP4 model. We thus provide a detailed ultra-structural evaluation of dorsal CST and motor neuron damage while putting emphasis on the relation between CNS pathology and clinical disease severity.

Materials and methods

Mice

Female C57BL/6 mice (6-8 weeks old) were purchased from Charles River (Sulzfeld, Germany) and maintained at our local animal facilities under specific pathogen-free conditions in IVC cages. All treatments complied with the institutional guidelines.

Induction and clinical assessment of EAE

MOG peptide was obtained from EZBiolab (Carmel, IN), and MP4 from Alexion Pharmaceuticals (Cheshire, CT). Incomplete Freund's adjuvant (IFA) was prepared as a 1:9 mixture of mannide monooleate (Sigma-Aldrich, St. Louis, MO) and paraffin oil (EMScience, Gibbstown, NJ), complete Freund's adjuvant (CFA) was obtained by mixing *Mycobacterium tuberculosis* H37 RA (Difco Laboratories, Franklin Lakes, NJ) at 5 mg/ml into IFA. Mice were immunized subcutaneously in both sides of the flank with a total dose of 100 μg MOG peptide or 150 μg MP4 emulsified in CFA. Pertussis toxin (PTX; List Biological Laboratories, Hornby, ONT, Canada) was given intraperitoneally at 200 ng per mouse on the day of immunization and 48 h later. Mice that did not receive any treatment or were immunized with PBS in CFA were used as controls. Clinical assessment of EAE was performed daily according to the standard EAE scale: (0), no disease; (1), floppy tail; (2), hind limb weakness; (3), full hind limb paralysis; (4), quadriplegia; (5), death. Mice that were in between the clear-cut gradations of clinical signs were scored intermediately in increments of 0.5. Mice were sacrificed during the plateau phase of the disease during which the clinical scores reached a maximum. For analysis of CST pathology, mice were subdivided into two main groups. Mild EAE encompassed the clinical scores 0.5-2, severe EAE referred to clinical scores >2. The mean clinical score in the MOG peptide and MP4 group was similar both in mild and severe EAE (1.35±0.24 versus 1.25±0.26 in

Table 1. Elapsed time in days from disease onset until tissue harvesting and terminal clinical score of individual mice.

	MOG peptide 35-55				MP4			
	mild		severe		mild		severe	
Mouse	elapsed time in days	terminal clinical score	elapsed time in days	terminal clinical score	elapsed time in days	terminal clinical score	elapsed time in days	terminal clinical score
1	14	1	42	2.5	172	1	157	2.5
2	41	1.5	27	3	137	1	166	2.5
3	137	1.5	84	3	136	1	24	3
4	187	1.5	84	2.5	110	1.5	169	2.5
5	109	1.5	84	2.5	35	1.5	20	2.5
6	27	1.5	98	2.5	25	1.5	178	3
7	168	1	220	2.5	161	1	187	2.5
8					36	1.5	25	2.5
Mean value ± SD	97.6±70.5	1.35±0.24	91.3±62.4	2.64±0.24	101.5±60.5	1.25±0.26	115.7±77.3	2.63±0.23

mild MOG peptide versus MP4-induced EAE with p=0.593 and 2.64±0.24 versus 2.63±0.23 in severe MOG peptide versus MP4-induced EAE with p=0.582) (Table 1). The elapsed time from disease onset until tissue-harvesting in the plateau phase of the disease when mice showed maximum scores was similar between all groups (MOGp mild: 97.6±70.5 days; MOGp severe: 91.3±62.4 days; MP4 mild: 101.5±60.5 days; MP4 severe: 115.7±77.3 days) and did not reach statistical significance (Table 1).

Electron microscopy

Mice were perfused intracardially with 4 % paraformaldehyde/4% glutaraldehyde in 0.1 M phosphate-buffered saline (pH=7.4). The tissue was post-fixed at 4°C for at least 24 h. Spinal cords were carefully removed from the vertebral canal. The lumbosacral part was cut off with sharp blades and post-fixed again for at least 24 h. Specimens were rinsed in cacodylate buffer three times and treated with 1 % osmium tetroxide for 4 h on ice. After repeated rinsing, the tissue was dehydrated in a graded series of ethanol and treated with 1% uranyl acetate in 70% ethanol for contrast enhancement overnight. Subsequently, specimens were embedded in epon (Serva Electrophoresis GmbH, Heidelberg, Germany) and polymerised at 60°C for at least 72 hours. Eighty nm thick ultrathin sections of each plastic-embedded spinal cord sample were cut on an ultramicrotome (Reichert, Bensheim, Germany). Swimming in the water trough of the diamond knife, the ultrathin sections were stretched with xylene vapour and thereafter carefully suspended on 150 mesh hexagonal Formvar-coated copper grids (Electron Microscopy Sciences, Hatfield, PA). The preparations were stained with 1% aqueous uranyl acetate solution for 20 minutes and Reynold's lead citrate solution for 7 minutes. Ten equidistant sections that covered the lumbosacral spinal cord from segments L1-S5 per mouse were examined with a Zeiss EM 902A transmission electron microscope at 80 kV acceleration voltage and images were taken with an EM digital camera system (MegaView, analysis© docu 3.2, Olympus Soft Imaging Systems GmbH, Münster, Germany). The examination was done by an observer blinded as to the sensitization and clinical status of the animals.

Immunohistochemistry

Staining for motor neuron perikarya was done on 7 μm thick frozen spinal cord sections. The tissue was fixed with ice-cold methanol. Neurofilament H non-phosphorylated SMI-32 antibody (Covance, Princeton, NJ) was used at 1:1000 dilution to stain motor neuron perikarya using the Vector M.O.M kit (Vector Labs, Burlingame, CA) according to the manufacturer's instructions. Sections were observed with a Zeiss Axioskop 50 epifluorescence microscope. For fluorescence detection the "rhodamine" filter (Nr. 15 of Carl Zeiss, excitation BP 546/12, beamsplitter FT 580, emission LP 590) and the "ultraviolet" filter (Nr. 1 of Carl Zeiss, excitation BP 365/12, Emission LP 397) were used. Digital images were acquired using a slow scan CCD camera (SPOT RT, Diagnostic Instruments, Sterling Heights) and software.

Statistical analysis

Student's t-test calculated with SigmaStat software (Version 7.0; SPSS, Chicago, IL) was used to determine the statistical significance of the differences in CNS pathology. Statistical significance was set at $p \leq 0.05$.

Results

Corticospinal tract degeneration is a consistent feature of MOGp- and MP4-induced EAE

Fig. 1 delineates the localization of the corticospinal tract (CST) in the lumbar part of the murine spinal cord (Fig. 1). The extent of CST pathology in MOG peptide- and MP4-induced EAE was assessed using a semi-quantitative scoring system, which included assessment of myelin and axonal morphology in addition to the integrity of the CNS interstitium (Fig. 2). Tissue with a score of 0 showed no pathological changes. A score of 1 delineated minor alterations, most frequently including dissociation of the CNS interstitium and slight deformations of the axonal shape, while myelin and axonal damage were not frequently found. A histology score of 2 related to progressive axonal injury that encompassed axonal swelling, a decrease in the nearest neighbor neurofilament distance (NNND), an increase in

Table 2. Semi-quantitative scoring system of white matter pathology.

White matter score	
0	no pathology
1	minor alterations, including dissociation of the CNS interstitium and slight deformations of the axonal shape
2	progressive axonal injury, including mitochondrial swelling, decrease in NNND, increase in the size of inner tongue formation and axonal swelling
3	extensive nerve fiber damage and degradation of the CNS interstitium with build-up of cellular debris from disrupted myelin and axons - up to 80 % of the tissue appeared pathological
4	up to 100 % of the tissue appeared pathological

the sizes of oligodendroglial inner tongue formation and mitochondrial swelling. A score of 3 described extensive nerve fiber damage and degradation of the CNS interstitium with the build-up of cellular debris from disrupted myelin and axons. Typically, in these mice up to 80% of the tissue appeared pathological. A score of 4 related to tissue that appeared completely pathologically altered. However, it should be noted that a score of 4 was rarely seen. The mean pathological score in relation to the clinical disease severity in MOG peptide- and MP4-induced EAE is shown in Fig. 3A. In mild EAE, both models showed a significant increase ($p<0.001$) in the mean pathological scores compared to control mice. There was no significant difference in the mean pathological score comparing MOGp- induced EAE to the MP4 model (2.22±0.5 compared to 1.83±0.4; $p=0.248$, Fig. 3A). Representative images are shown in Fig. 3B,C and E. In the severe cases of the disease we observed a further significant increase in the mean pathological score compared to controls ($p<0.001$) in both models (Fig. 3A,D,F). MOGp-immunized mice showed a mean score of 3.1±0.34 compared to 2.2±0.37 in the MP4 model ($p=0.01$).

The extent of myelin pathology reflects clinical disease severity

Having assessed the mean pathological score, which takes into account the tissue as a whole, we examined several structures in greater detail. As shown in Fig. 4A we found a significant increase ($p<0.001$) in CST myelin damage from mild to severe EAE in both models. For the evaluation of myelin pathology, all myelin sheaths were examined and classified as "normal appearing" versus "damaged". "Normal appearing" myelin was characterized by a homogeneous, uninterrupted, non-dispersed structure with the myelin lamellae being clearly visible at high magnification (Fig. 4B). "Damaged" myelin ranged from occasional structural loosening to complete degeneration of the myelin sheath (Fig. 4C-F). In contrast to the control group, in which only 5.0±2.5% of the nerve fibers showed signs of myelin pathology or damage (Fig. 4A,B), the mild course of EAE was already characterized by a significant increase in myelin damage, reaching 68.0±14.1% in the MP4- and 77.0±18.3% in MOGp-induced EAE (Fig. 4A,C,E). The difference between the MOG peptide and MP4 group was not statistically significant ($p=0.438$). With increasing severity of the disease we found a further increase in myelin damage. In MP4-immunized mice that displayed severe EAE 85.0±13.4% of CST myelin sheaths were pathological (Fig. 4A,F) compared to 95.0±0.9% in the MOG peptide model ($p=0.378$, Fig. 4A,D). Overall, it should be noted that the MOG peptide model frequently encompassed axons with altered organelles reflected by dark degeneration, as well as axons with massive spheroids indicative of spinal degeneration.

Mitochondrial swelling, an increase in inner tongue formation and a decrease in NNND are morphological correlates of axonal damage

Studies of the axoplasm showed differences in morphological characteristics between the MOG peptide and MP4 model. At a 12000x magnification we

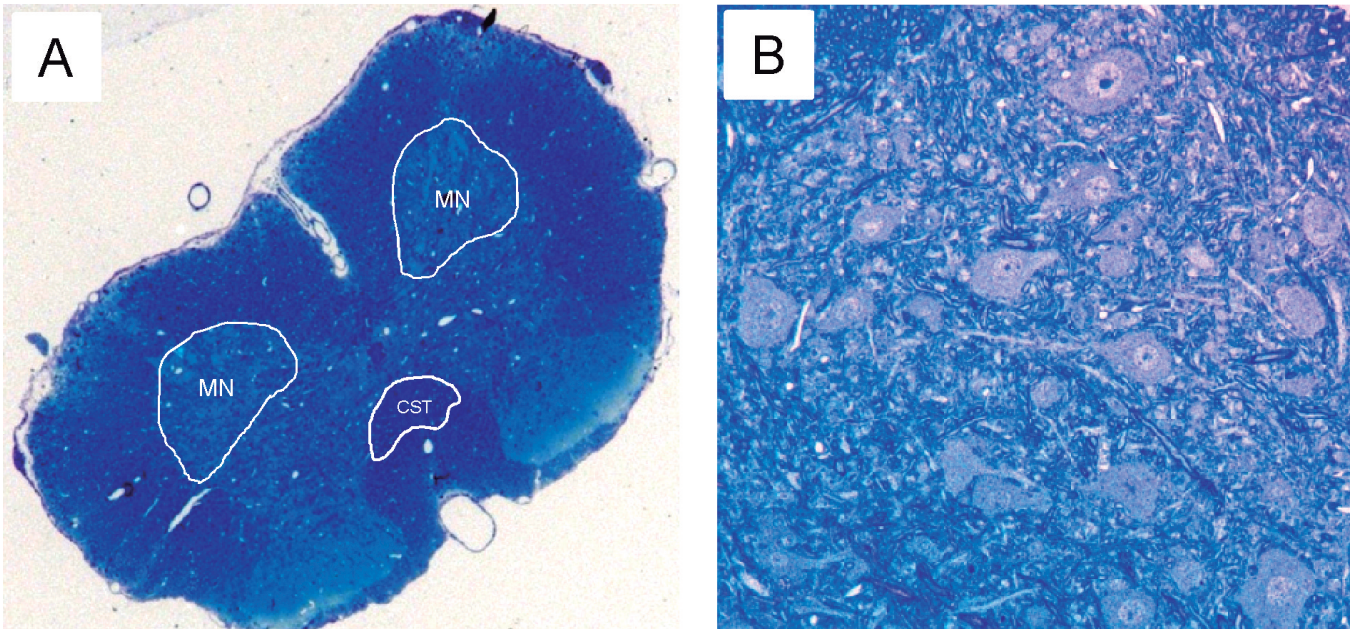

Fig. 1. Localization of corticospinal tract (CST) and motor neurons (MN) in the murine spinal cord. The image shows a methylene blue-stained transverse section of murine lumbar spinal cord. **A**. The CST and the anterior horns containing the motor neurons are circled at 40x. The anterior horn is shown at 200x magnification in panel **B**.

examined the axonal components mitochondria, neurofilaments and inner tongues. Mitochondria were examined by calculating the percentage of the mitochondrial area in relation to the total axonal area (Fig. 5A-D). While in the MOG peptide model a significant increase in mitochondrial size was evident in severe EAE compared to the control group ($p<0.001$), mitochondrial swelling was absent in MP4-induced

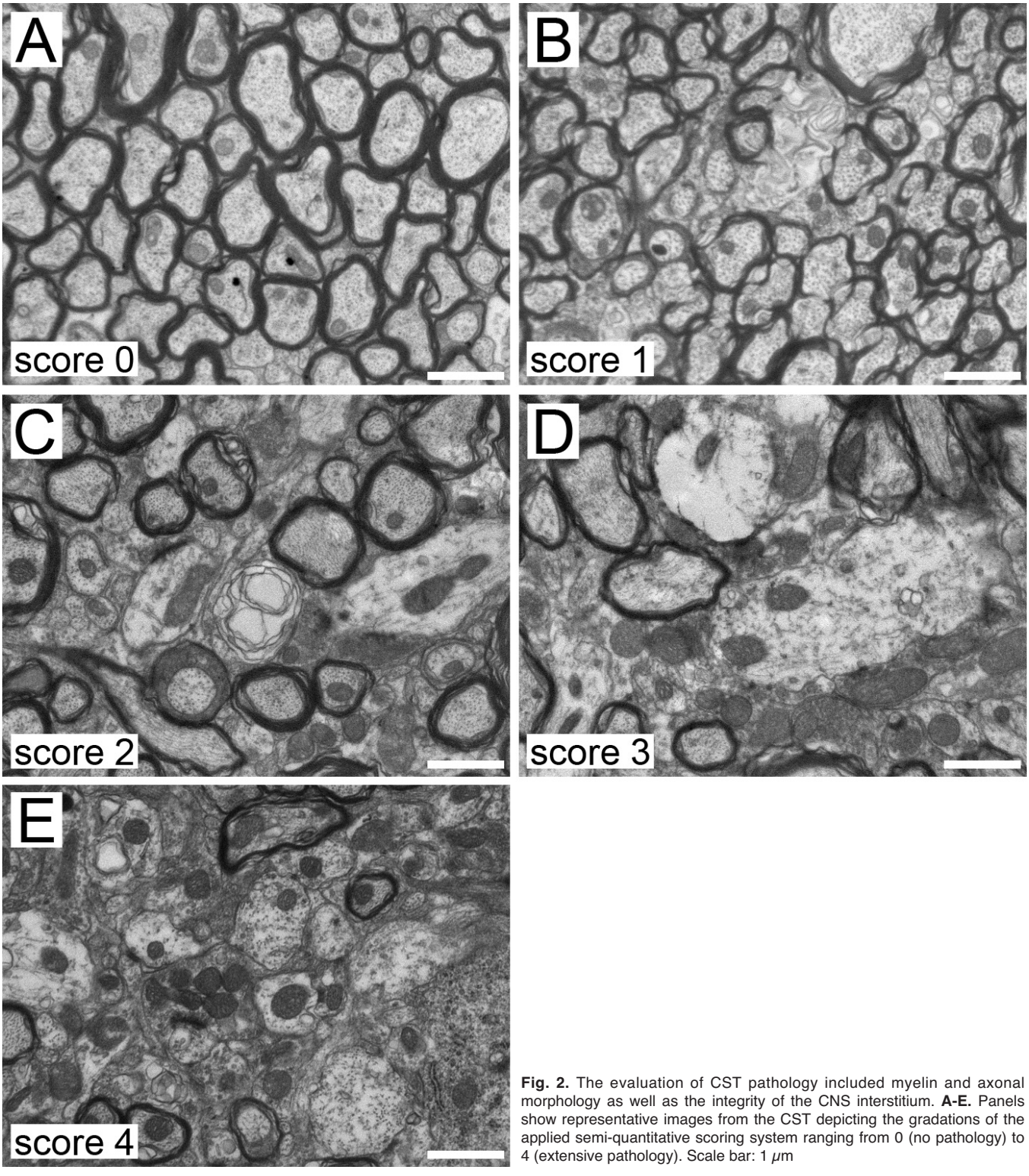

Fig. 2. The evaluation of CST pathology included myelin and axonal morphology as well as the integrity of the CNS interstitium. **A-E.** Panels show representative images from the CST depicting the gradations of the applied semi-quantitative scoring system ranging from 0 (no pathology) to 4 (extensive pathology). Scale bar: 1 μm

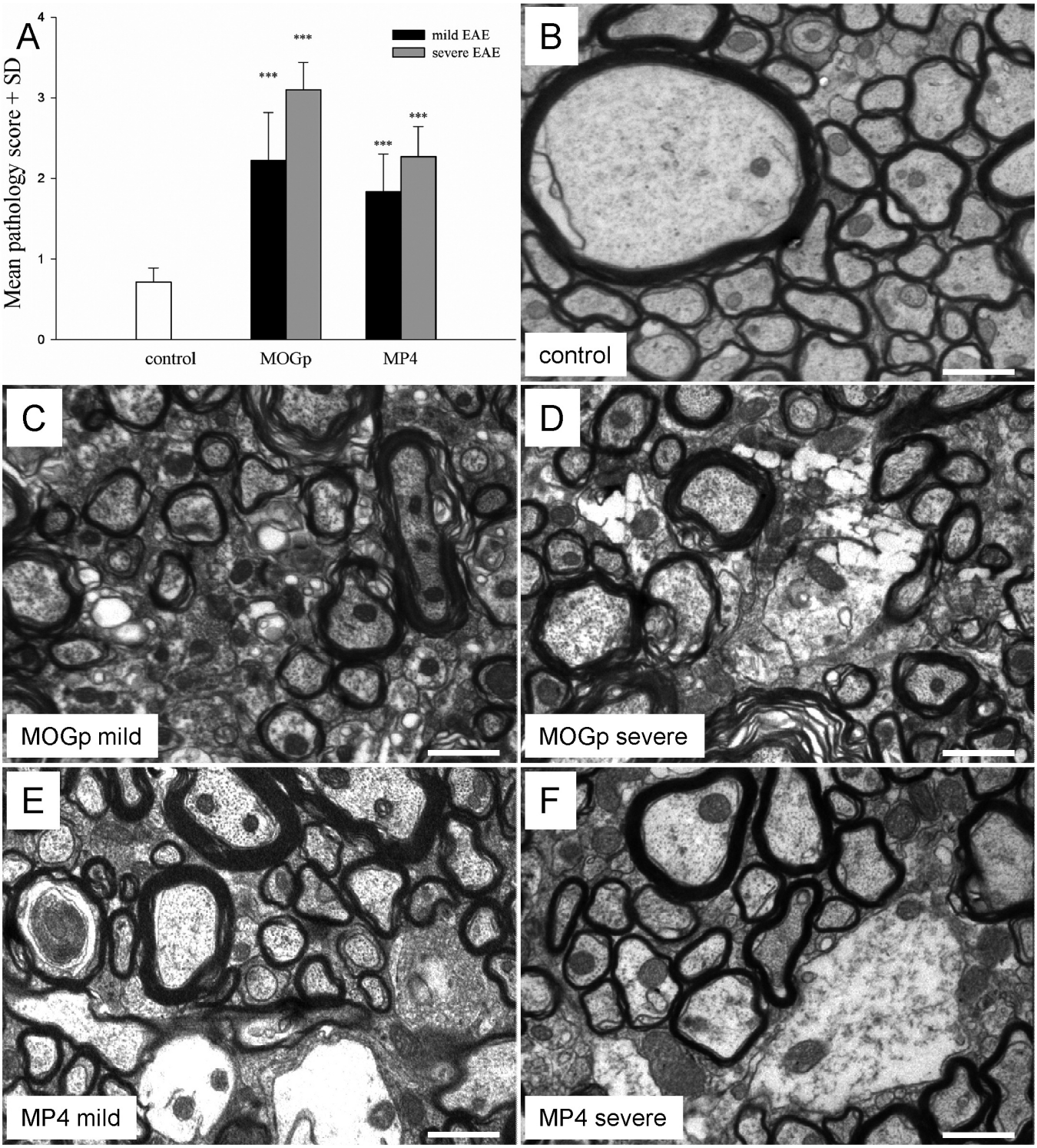

Fig. 3. CST pathology is evident in both MOG peptide- and MP4-induced EAE. CST pathology was assessed using a semi-quantitative scoring system. **A.** Mean pathology score ± SD in mild and severe MOG peptide versus MP4-induced EAE compared to control animals. **B-F.** Representative electron microscopic images. The data refer to n=6-8 mice tested in each group and tested in at least 3 independent experiments. *** $p \leq 0.001$ compared to the controls. Scale bar: 1 μm

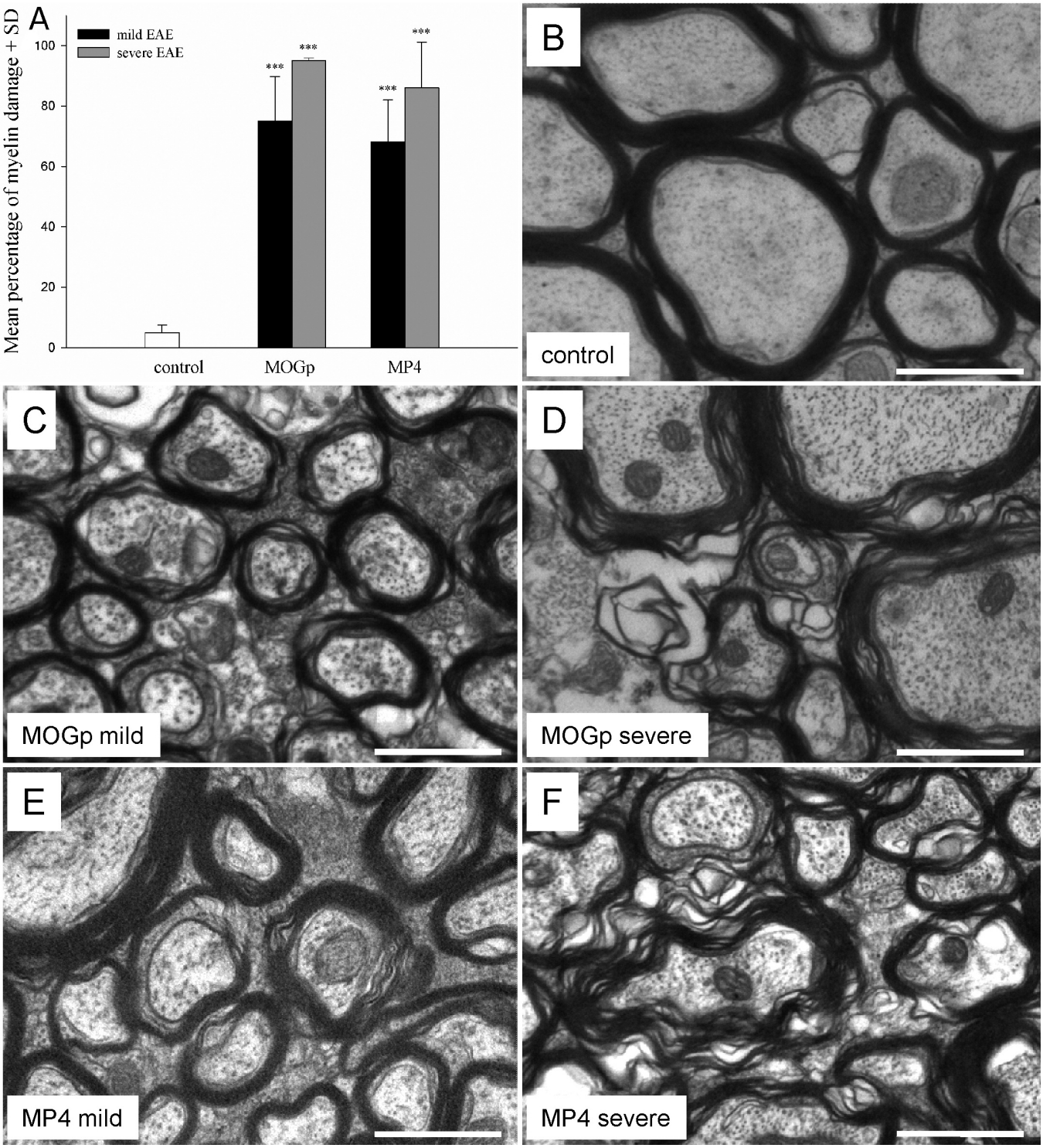

Fig. 4. In MOG peptide- and MP4-induced EAE CST myelin pathology is associated with clinical disease severity. The extent of myelin damage was assessed and put in relation to the total number of nerve fibers in the CST. **A.** Mean percentage of myelin damage ± SD in mild and severe MOG peptide versus MP4-induced EAE compared to control animals. **B-F.** Representative electron microscopic images. The data refer to n=6-8 mice tested in each group and tested in at least 3 independent experiments. *** p≤0.001 compared to the controls. Scale bar: 1 μm

EAE. Next, we evaluated the NNND (Fig. 5E-H). Both models, MOG peptide- and MP4-induced EAE showed a significant decrease in NNND compared to the control group in mild EAE ($p<0.001$ and $p=0.01$, respectively). In severe EAE, the NNND remained significantly decreased only in the MOGp group ($p<0.001$). In addition, the MOGp model was characterized by a significant increase in inner tongue area that was 2-fold higher than in the control group in mild EAE ($p<0.001$, Fig. 5J,K). In severe EAE inner tongue formation recessed, but remained elevated compared to the control group ($p=0.002$, Fig. 5I). In MP4-induced EAE we found a significant increase in inner tongue area in both mild and severe EAE compared to the controls ($p<0.001$, Fig. 5I,J,L).

The extent of motor neuron pathology is CNS antigen-dependent in EAE

In addition to CST pathology, we also evaluated motor neuron degeneration (for orientation see Fig. 1). Our analysis was focused on the occurrence of intracytoplasmic vacuoles, changes in the rough endoplasmic reticulum (rER) and the nucleus, and the number of synapses per mm (Fig. 6). For analysis of the number of synapses and rER changes the quantity was assessed semi-quantitatively from 0 (none) to +++ (abundant), while the other parameters were evaluated using a semi-quantitative scoring system ranging from 0 (absence of degeneration) to +++ (severe pathology). Our data show only mild motor neuron degeneration in MOGp-immunized mice, characterized by an increased number of intracytoplasmic vacuoles (Fig. 6C) and slight nuclear changes that encompassed an irregular undulation of the nuclear membrane (Fig. 6I). MP4-induced EAE in contrast led to more severe nuclear membrane defects up to complete nucleic resolution (Fig. 6J). The extent of rER alterations and the number of synapses remained largely unchanged compared to the control group (Fig. 6A-D). Only in severe MP4-induced EAE we noted a beginning disintegration of the rER (Fig. 6A,D). The number of synapses per mm was decreased in both MOGp- and MP4-induced EAE compared to controls. Besides the analysis of motor neuron alterations on the ultrastructural level, motor neuron atrophy was assessed by immunohistochemical staining of hypophosphorylated neurofilament H. It was observed both in MOGp- and MP4-induced EAE, while

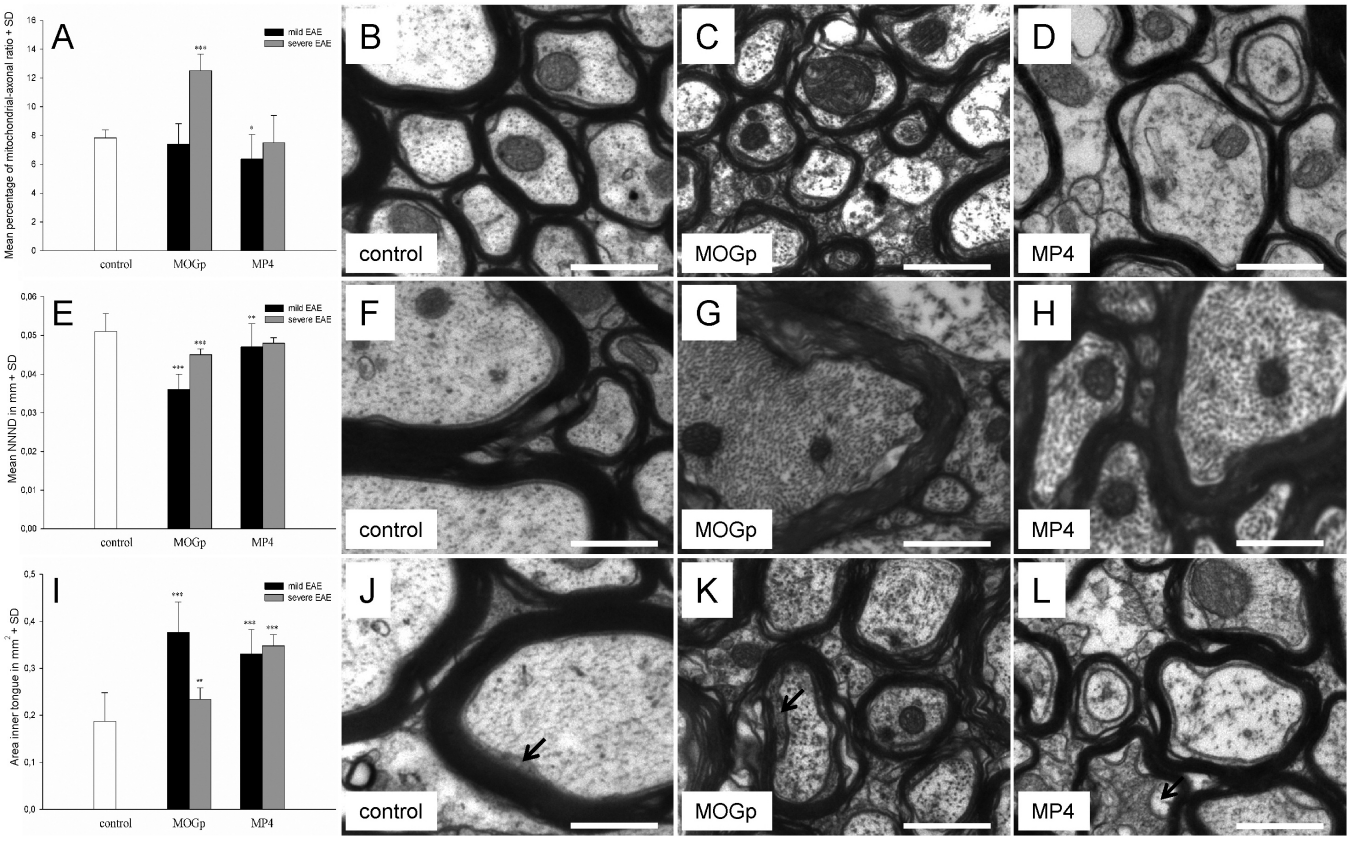

Fig. 5. Features of axonal damage in MOG peptide- and MP4-induced EAE. Axonal damage comprised mitochondrial swelling (**A-D),** a decrease in NNND **(E-H)** and an increase in inner tongue size **(I-L**). Arrows indicate inner tongues in panels **(J-L)**. **A, E, I**. Mean values ± SD for mild and severe MOG peptide- and MP4-induced EAE compared to control animals. The data refer to n=6-8 mice tested in each group and tested in at least 3 independent experiments. * $p=0.05$, ** $0.049<p>0.002$, *** $p \leq 0.001$ compared to the controls. Scale bar: 1 μm

A

	degeneration	vacuoles	nuclear changes	rough ER	synapses per mm
CTRL	0	0	0	++	+++
MOG mild	+	+	+	++	++
MOG severe	+	+	+	++	++
MP4 mild	++	++	+++	++	++
MP4 severe	++	++	+++	+	++

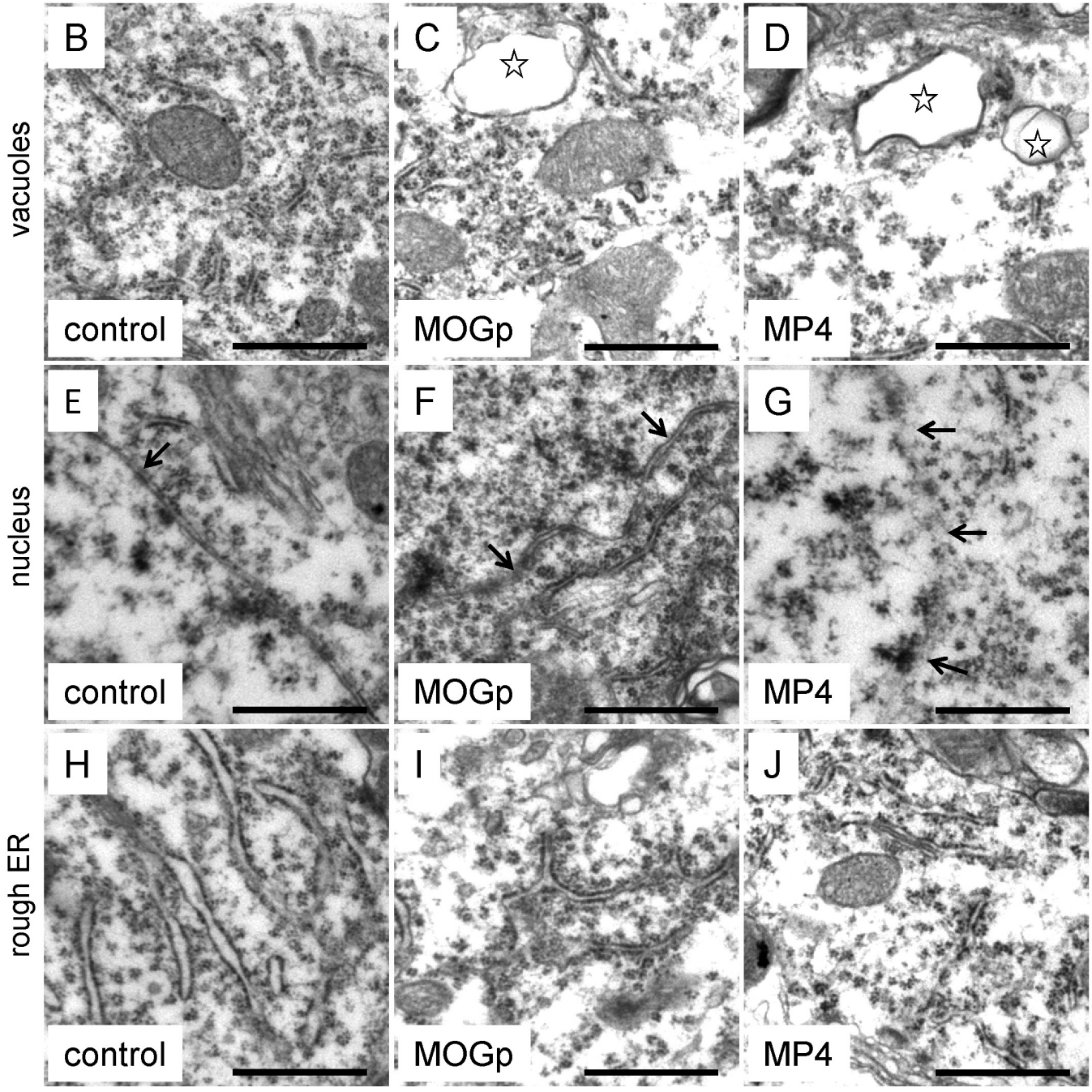

Fig. 6. MP4-induced EAE displays severe motor neuron pathology. **A.** Motor neuron pathology was assessed using a semi-quantitative scoring system, which considered the overall degree of motor neuron degeneration, the occurrence of intracytoplasmic vacuoles **(B-D)**, rough ER **(E-G)** and nuclear changes **(H-J)**, as well as the number of synapses per mm. Stars in panels **F** and **G** designate vacuoles, the arrows in panels **I** and **J** indicate the nuclear membrane. The data refer to n=6-8 mice tested in each group and tested in at least 3 independent experiments. Scale bar: 1 μm.

being more pronounced in the latter model (Fig. 7).

Discussion

Clinically, EAE is characterized by the manifestation of motor deficits (Lublin et al., 1981; Wujek et al., 2002). However, direct studies of corticospinal tract and motor neuron pathology that could explain the functional deficits are scarce. Focus has rather been laid on general assessments of CNS histopathology, while specific evaluations of individual fiber tracts have not been extensively done. Our study was intended to further investigate the relationship between morphological changes in the CST and motor neurons of MOG peptide- and MP4-induced EAE and the clinical deficits of the mice.

In our previous studies, we analyzed corticospinal tract pathology by using light microscopy. While we did not observe any CST alterations in the MP4 model, results for the MOG peptide model were differential and the extent of CST pathologies ranged from 27% in acute and 0% in chronic EAE (Recks et al., 2011) to 80% (acute) and 40% (chronic) (Kuerten et al., 2011b). While in the first study, pathology was restricted to the acute stage of the disease and characterized by inflammatory infiltrates and parenchymal edema in the absence of neurodegeneration, pathologic features in the latter study comprised inflammation, demyelination and axolysis (Kuerten et al., 2011b; Recks et al., 2011). The results from our present study were acquired by using electron microscopy and delineate that CST degeneration is a consistent feature of both MOGp- and MP4-induced EAE, which depicts the importance of ultrastructural studies for in-depth assessment of CNS histopathology in EAE. In line with data from MS patients that show a strong correlation between the extent of neurodegeneration and disease severity (De Stefano et al., 1998; Trapp et al., 1998), our results confirm the assumption that increasing myelin and axonal damage is associated with increasing severity of paralysis in MOGp- and MP4-induced EAE.

In the present study, we found distinct features of axonal pathology in both models, including mitochondrial swelling, a decrease in NNND and an increase in inner tongue formation. All of these features have been suggested before to be correlates of axonal damage (Herrero-Herranz et al., 2008; Jones et al., 2008; Soulika et al., 2009). Mitochondrial swelling is regarded as an early sign of axonal dysfunction resulting from permeability transition due to a pathological activation of the mitochondrial permeability transition pore (Baines et al., 2005; Nakagawa et al., 2005; Mao and Reddy, 2010). In addition, Lunn et al. suggested the NNND as a feature of axonal pathology since it was reduced in damaged compared to normal axons (Lunn et al., 2002). The axon diameter is determined by its neurofilament numbers and the NNND depends on the phosphorylation status of neurofilament sidearms. An increase in inner tongue formation is considered to be the result of oligodendrocyte swelling, which displaces the axoplasm and creates an additional space between axon and myelin sheath (Lappe-Siefke et al, 2003; Morfini et al., 2009). The inner tongue has been suggested to play the predominant role during the removal of the axon, and inner tongue swelling has been considered to be a feature of early axonal disruption (Cook and Wiesniewski, 1973). In contrast to initial theories about MS pathology, it has been shown that axonal injury can

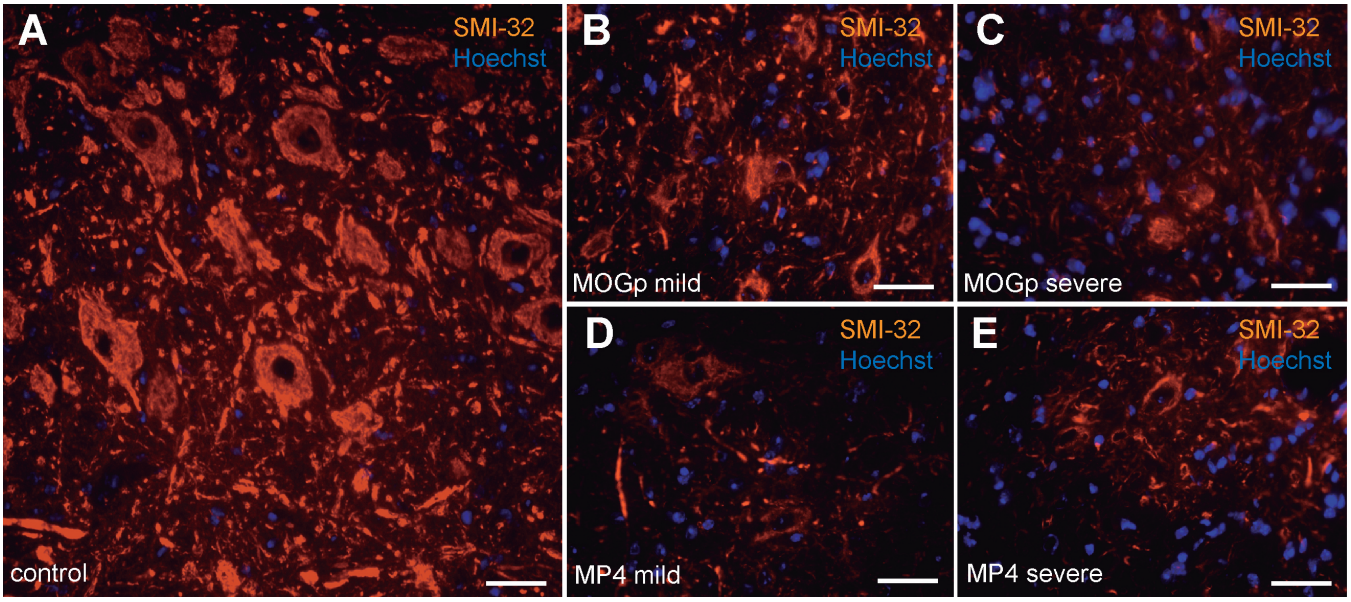

Fig. 7. Motor neuron atrophy in MP4- and MOG peptide-induced EAE. Seven μm thick lumbar spinal cord sections of control **(A)**, MOG peptide- **(B, C)** and MP4-immunized **(D, E)** mice were stained with SMI-32 antibody and the motor neuron phenotype was analyzed. Scale bar: 20 μm

occur early on in the disease and independently from myelin damage (Tsunoda and Fujinami, 2002; Trapp, 2004; Comi, 2009). In the present study, we found evidence for axonal alterations in the absence of myelin abnormalities, reinforcing the revised concept of MS pathology.

In addition to white matter pathology, motor neuron pathology as an aspect of gray matter disease has been investigated in several studies in both MS and EAE. Vogt and colleagues found a massive loss of lower motor neurons in MS patients, which was indicated by a decrease in compound muscle action potential amplitudes and motor unit numbers in MS patients compared to control subjects (Vogt et al., 2009). The data was confirmed by high-precision unbiased stereological quantification of spinal cord neurons in *post-mortem* MS tissue. In this material, T cells secreting TNF-related apoptosis inducing ligand TRAIL were found in close vicinity to apoptotic neurons (Vogt et al., 2009). These findings prompted them to further investigate this phenomenon in MOGp-elicited EAE where they observed a comparable, TRAIL-dependent loss in the numbers of motor neurons (Vogt et al., 2009). Equally, Aharoni et al. found a significant reduction in the number of lower motor neurons in this model, with motor neuron loss being most prominent in the chronic stage of the disease (Aharoni et al., 2011). In contrast, Bannerman et al. have reported motor neuron atrophy but not loss in MOGp-induced EAE of C57BL/6 mice by staining of hypophosphorylated neurofilament H (Bannerman et al., 2005). In agreement with this study, we did not observe motor neuron apoptosis but rather found significant alterations in the motor neuron perikaryal phosphorylation in both MOG peptide- and MP4-induced EAE (Kuerten et al., 2011b). Atrophy visualized by hypophosphorylated neurofilament heavy (hypoP-NF-H) immunohistology was transient in MOGp-elicited EAE (Bannerman et al., 2005; Kuerten et al., 2011b), while we found more permanent motor neuron alterations in MP4-induced EAE (Kuerten et al., 2011b). In addition, Bannerman and colleagues also observed chronic alterations in the architecture of motor neuron dendrites, including dendritic thinning, shortening and fragmentation throughout the course of MOGp-induced EAE. Clearly, the cause of these alterations remains to be elucidated and additional studies in the animal model are needed to identify the mechanisms that account for the important aspects of gray matter pathology in the human disease. The present study has been carried out to work towards this aim. We were able to reproduce the crucial feature of gray matter pathology in both MOG peptide- and MP4-induced EAE. However, motor neuron degeneration was much less pronounced in the MOG peptide compared to the MP4 model. Considering this differential targeting of CST and motor neurons in the two models, our data underline that the CNS antigen triggering the autoimmune response is decisive for the resulting histological outcome.

In conclusion, the present study has shown that besides inflammation and demyelination, axonal damage and gray matter pathology are important attributes of the EAE model. While our data clearly affirm score-dependent changes in CST and motor neuron pathology, we did not take into account variations emerging from different disease stages. In order to characterize the contribution of specific pathological mechanisms such as CST and/or motor neuron pathology more closely, it is essential to establish clear kinetics in order to identify the underlying primary mechanisms - future studies will have to address this issue. Finally, our results delineate that both the MOG peptide and the MP4 model are valuable tools for MS research since both represent (to a different extent) important aspects of the human disease. Our data also corroborate that our understanding of MS pathology needs to be extended to include gray matter pathology as a crucial feature beyond the traditional white matter paradigm.

Acknowledgements. We would like to thank J. Kozlowski, C. Hoffmann and E. Janßen for technical support. Support was provided by the German Research Foundation (DFG) grant KU 2760/2-1, the Koeln Fortune Programm and the Imhoff-Stiftung (grants to S.K.). T.L.G. and M.R. contributed equally to this work.

Disclosures. None of the authors has any conflict of interest.

Referenes

Aharoni R., Vainshtein A., Stock A., Eilam R., From R., Shinder V. and Arnon R. (2011). Distinct pathological patterns in relapsing-remitting and chronic models of experimental autoimmune enchephalomyelitis and the neuroprotective effect of glatiramer acetate. J. Autoimmun. 37, 228-241.

Baines C.P., Kaiser R.A., Purcell N.H., Blair N.S., Osinska H., Hambleton M.A., Brunskill E.W., Sayen M.R., Gottlieb R.A., Dorn G.W., Robbins J. and Molkentin J.D. (2005). Loss of cyclophilin D reveals a critical role for mitochondrial permeability transition in cell death. Nature 434, 658-662.

Bannerman P.G., Hahn A., Ramirez S., Morley M., Bönnemann C., Yu S., Zhang G.X., Rostami A. and Pleasure D. (2005). Motor neuron pathology in experimental autoimmune encephalomyelitis: studies in THY1-YFP transgenic mice. Brain 128, 1877-1886.

Bernard C.C., Johns T.G., Slavin A., Ichikawa M., Ewing C., Liu J. and Bettadapura J. (1997). Myelin oligodendrocyte glycoprotein: a novel candidate autoantigen in multiple sclerosis. J. Mol. Med. 75, 77-88.

Bitsch A., Schuchardt J., Bunkowski S., Kuhlmann T. and Brück W. (2000). Acute axonal injury in multiple sclerosis. Correlation with demyelination and inflammation. Brain 123, 1174-1183.

Calabrese M., Filippi M. and Gallo P. (2010). Cortical lesions in multiple sclerosis. Nat. Rev. Neurol. 6, 438-444.

Comi G. (2009). Shifting the paradigm toward earlier treatment of multiple sclerosis with interferon beta. Clin. Ther. 31, 1142-1157.

Cook D.C. and Wisnieswksi H.M. (1973). The role of oligodendroglia and astroglia in Wallerian degeneration of the optic nerve. Brain Res. 61, 191-206.

De Stefano N., Matthews P.M., Fu L., Narayanan S., Stanley J., Francis G.S., Antel J.P. and Arnold D.L. (1998). Axonal damage correlates with disability in patients with relapsing-remitting multiple sclerosis. Results of a longitudinal magnetic resonance spectroscopy study.

Brain 121, 1469-1477.

Gold R., Linington C. and Lassmann H. (2006). Understanding pathogenesis and therapy of multiple sclerosis via animal models: 70 years of merits and culprits in experimental autoimmune encephalomyelitis research. Brain 129, 1953-1971.

Goverman J. and Brabb T. (1996). Rodent models of experimental allergic encephalomyelitis applied to the study of multiple sclerosis. Lab. Anim. Sci. 46, 482-492.

Handel A.E., Lincoln M.R. and Ramagopalan S.V. (2011). Of mice and men: experimental autoimmune encephalitis and multiple sclerosis. Eur. J. Clin. Invest. 41, 1254-1258.

Herrero-Herranz E., Pardok L.A., Gold R. and Linker R.A. (2008). Pattern of axonal injury in murine myelin oligodendrocyte glycoprotein induced experimental autoimmune encephalomyelitis: implications for multiple sclerosis. Neurobiol. Dis. 30, 162-173.

Kuerten S., Lichtenegger F.S., Faas S., Angelov D.N., Tary-Lehmann M. and Lehmann P.V. (2006). MBP-PLP fusion protein-induced EAE in C57BL/6 mice. J. Neuroimmunol. 178, 4749-4756.

Kuerten S., Kostova-Bales D.A., Frenzel L.P., Tigno J.T., Tary-Lehmann M., Angelov D.N. and Lehmann P.V. (2007). MP4-, and MOG:35-55-induced EAE in C57BL/6 mice differentially targets brain, spinal cord and cerebellum. J. Neuroimmunol. 189, 31-40.

Kuerten S., Javeri S., Tary-Lehmann M., Lehmann P.V. and Angelov D.N. (2008). Fundamental differences in the dynamics of CNS lesion development and composition in MP4-, and MOG peptide 35-55-inuced experimental autoimmune encephalomyelitis. Clin. Immunol. 129, 256-267.

Kuerten S., Pauly R., Rottlaender A., Rodi M., Gruppe T.L., Addicks K., Tary-Lehmann M. and Lehmann P.V. (2011a). Myelin-reactive antibodies mediate the pathology of MBP-PLP fusion protein MP4-induced EAE. Clin. Immunol. 140, 54-62.

Kuerten S., Gruppe T.L., Laurentius L.M., Kirch C., Tary-Lehmann M., Lehmann P.V. and Addicks K. (2011b). Differential patterns of spinal cord pathology induced by MP4, MOG peptide 35-55, and PLP 178-191 in C57BL/6 mice. APMIS 119, 336-346.

Jones M.V., Nguyen T.T., Deboy C.A., Griffin J.W., Whartenby K.A., Kerr D.A. and Calabresi P.A. (2008). Behavioral and pathological outcomes in MOG 35-55 experimental autoimmune encephalomyelitis. J. Neuroimmunol. 199, 83-93.

Lappe-Siefke C., Goebbels S., Gravel M., Nicksch E., Lee J., Braun P.E., Griffiths I.R. and Nave KA. (2003). Disruption of Cnp1 uncouples oligodendroglial functions in axonal support and myelination. Nat. Genet. 3, 366-374

Lassmann H., Brück W. and Lucchinetti C.F. (2007). The immunopathology of multiple sclerosis: an overview. Brain Pathol. 17, 210-218.

Lublin F.D., Maurer P.H., Berry R.G. and Tippett D. (1981). Delayed, relapsing experimental allergic encephalomyelitis in mice. J. Immunol. 126, 819-822.

Lunn M.P.T., Crawford T.O., Hughes R.A.C., Griffin J.W. and Sheikh K.A. (2002). Anti-myelin-associated glycoprotein antibodies alter neurofilament spacing. Brain 125, 904-911.

Mao P. and Reddy P.H. (2010). Is multiple sclerosis a mitochondrial disease? Biochim. Biophys. Acta 1802, 66-79.

Mendel I., Kerlero de Rosbo N. and Ben-Nun A. (1995). A myelin oligodendrocyte glycoprotein peptide induces typical chronic experimental autoimmune encephalomyelitis in H-2b mice: fine specificity and T cell receptor V beta expression of encephalitogenic T cells. Eur. J. Immunol. 25, 1951-1959.

Morfini G.A., Burns M., Binder L.I., Kanaan N.M., LaPointe N., Bosco D.A., Brown H., Tiwari A., Hayward L., Edgar J., Nave K.A., Garberrn J., Atagi Y., Song Y., Pigino G. and Brady S.T. (2009). Axonal transport defects in neurodegenerative diseases. J. Neurosci. 29, 12776-12786.

Nakagawa T., Shimizu S., Watanabe T., Yamaguchi O., Otsu K., Yamagata H., Inohara H., Kubo T. and Tsujimoto Y. (2005). Cyclophilin D-dependent mitochondrial perme- ability transition regulates some necrotic but not apoptotic cell death. Nature 434, 652-658.

Oliver A.R., Lyon G.M. and Ruddle N.H. (2003). Rat and human myelin oligodendrocyte glycoproteins induce experimental autoimmune encephalomyelitis by different mechanisms in C57BL/6 mice. J. Immunol. 171, 462-468.

Recks M.S., Addicks K. and Kuerten S. (2011). Spinal cord histopathology of MOG peptide 35-55-induced experimental autoimmune encephalomyelitis is time- and score-dependent. Neurosci. Lett. 494, 227-231.

Soulika A.M., Lee E., McCauley E., Miers L., Bannerman P. and Pleasure D. (2009). Initiation and progression of axonopathy in experimental autoimmune encephalomyelitis. J. Neurosci. 29, 14965-14979.

Sospedra M. and Martin R. (2005). Immunology of multiple sclerosis. Annu. Rev. Immunol. 23, 683-747.

Steinman L. and Zamvil S.S. (2006). How to successfully apply animal studies in experimental allergic encephalomyelitis to research on multiple sclerosis. Ann. Neurol. 60, 12-21.

Tompkins S.M., Padilla J., Dal Canto M.C., Ting J.P., Van Kaer L. and Miller S.D. (2002). De novo central nervous system processing of myelin antigen is required for the initiation of experimental autoimmune encephalomyelitis. J. Immunol. 168, 4173-4183.

Trapp B.D., Peterson J., Ransohoff R.M., Rudick R., Mörk S. and Bö L. (1998). Axonal transection in the lesions of multiple sclerosis. N. Engl. J. Med. 338, 278-285.

Trapp B.D. (2004). Mechanisms of axonal loss and neuronal dysfunction in MS. Adv. Stud. Med. 4, S312-S315.

Tsunoda I. and Fujinami R.S. (2002). Inside-Out versus Outside-In models for virus induced demyelination: axonal damage triggering demyelination. Springer Semin. Immunopathol. 24, 105-125.

Vogt J., Paul F., Aktas O., Müller-Wielsch K., Dörr J., Dörr S., Bharathi B.S., Glumm R., Schmitz C., Steinbusch H., Raine C.S., Tsokos M., Nitsch R. and Zipp F. (2009). Lower motor neuron loss in multiple sclerosis and experimental autoimmune encephalomyelitis. Ann. Neurol. 66, 310-322.

Wujek J.R., Bjartmar C., Richer E., Ransohoff R.M., Yu M., Tuohy V.K. and Trapp B.D. (2002). Axon loss in the spinal cord determines permanent neurological disability in an animal model of multiple sclerosis. J. Neuropathol. Exp. Neurol. 61, 23-32.

Accepted March 23, 2012